

ACCEPTED MANUSCRIPT

Remote sensing of blood oxygenation using red-eye pupil reflection

To cite this article before publication: Tushar R Choudhary *et al* 2019 *Physiol. Meas.* in press <https://doi.org/10.1088/1361-6579/ab5f3b>

Manuscript version: Accepted Manuscript

Accepted Manuscript is “the version of the article accepted for publication including all changes made as a result of the peer review process, and which may also include the addition to the article by IOP Publishing of a header, an article ID, a cover sheet and/or an ‘Accepted Manuscript’ watermark, but excluding any other editing, typesetting or other changes made by IOP Publishing and/or its licensors”

This Accepted Manuscript is © 2019 Institute of Physics and Engineering in Medicine.

During the embargo period (the 12 month period from the publication of the Version of Record of this article), the Accepted Manuscript is fully protected by copyright and cannot be reused or reposted elsewhere.

As the Version of Record of this article is going to be / has been published on a subscription basis, this Accepted Manuscript is available for reuse under a CC BY-NC-ND 3.0 licence after the 12 month embargo period.

After the embargo period, everyone is permitted to use copy and redistribute this article for non-commercial purposes only, provided that they adhere to all the terms of the licence <https://creativecommons.org/licenses/by-nc-nd/3.0>

Although reasonable endeavours have been taken to obtain all necessary permissions from third parties to include their copyrighted content within this article, their full citation and copyright line may not be present in this Accepted Manuscript version. Before using any content from this article, please refer to the Version of Record on IOPscience once published for full citation and copyright details, as permissions will likely be required. All third party content is fully copyright protected, unless specifically stated otherwise in the figure caption in the Version of Record.

View the [article online](#) for updates and enhancements.

1 Remote sensing of blood oxygenation using red-eye pupil 2 reflection

3 **Tushar R. Choudhary**^{*,1,2}, **Derek Ball**⁴, **Javier Fernandez Ramos**², **Einar Stefansson**³,
4 **Andrew R. Harvey**²

5 ¹ The Roslin Institute and Royal (Dick) School of Veterinary Studies, University of Edinburgh,
6 Edinburgh, Midlothian, EH25 9RG. United Kingdom.

7 ² School of Physics and Astronomy, University of Glasgow, Glasgow, U.K.

8 ³ University of Iceland, Landspítali - The National University Hospital of Iceland

9 ⁴ Institute of Medical Education in Medical and Dental Sciences, University of Aberdeen,
10 Aberdeen, UK

11 * Corresponding Author

12 **Keywords:** Optical density ratio, spectral imaging, choroid, oxygen

13 Abstract

14 **Objective:** To develop a technique for remote sensing of systemic blood oxygenation using
15 red-eye pupil reflection.

16 **Approach:** The ratio of the intensities of light from the bright pupil reflections at oxygen
17 sensitive and isosbestic wavelengths is shown to be sensitive to the oxygenation of blood in
18 the eye. A conventional retinal camera, fitted with an Image Replicating Imaging
19 Spectrometer, was used at standoff range to record snapshot spectral images of the face and
20 eyes at eight different wavelengths. In our pilot study we measured optical-density ratios
21 (ODRs) of pupil reflections at wavelengths of 780nm and 800nm, simultaneous with pulse
22 oximetry, for ten healthy human subjects under conditions of normoxia and mild hypoxia
23 (15% oxygen). The low absorption at these infrared wavelengths localises the sensing to the
24 choroid. We propose that this can be used for as a proxy for systemic oximetry.

25 **Main results:** A significant reduction ($P < 0.001$) in ODR of the pupil images was observed
26 during hypoxia and returned to baseline on resumption of normoxia. We demonstrate that
27 measurement of the choroidal ODR can be used to detect changes in blood oxygenation that
28 correlate positively with pulse oximetry and with a noise-equivalent oximetry precision of
29 0.5%.

30 **Significance:** We describe a new method to remotely and non-invasively sense the oxygen
31 saturation of choroidal blood. The methodology provides a proxy for remote sensing of
32 cerebral and systemic blood oxygenation. We demonstrate the technique at short range but it
33 has potential for systemic oximetry at large standoff ranges.

37 1. Introduction

38 The retina has a particularly high metabolic demand for oxygen, which that is met mainly by
39 the choroid (about 85%) with the retinal circulation providing the remaining 15% [1, 2]. The
40 choroid supplies the outer layers of the retina including the photoreceptors while the inner
41 layers of the retina, including the retinal ganglion cells, are supplied by the retinal vessels. The
42 choroid is supplied with blood by the ophthalmic artery, which is a branch of the internal
43 carotid artery, and as such is considered to be a part of the cerebral vasculature [3]. Choroidal
44 vessels (arteries and venules) have a very high oxygen tension and a very low arteriovenous
45 oxygen saturation difference, in the region of about 3% [4]. It is possible, with traditional
46 spectrophotometric methods, to assess and study oxygen saturation in retinal vessels non-
47 invasively [5-8] or invasively through the application of phosphor into the circulation [9, 10]
48 or direct measurement through the use of an oxygen electrode [11]. We report a technique that
49 operates at standoff and non-invasively and so offers particular advantages as a technique for
50 routine sensing of choroidal oxygenation in humans. Our technique provides sensitive sensing
51 of blood oxygenation and can be further developed for measurement of absolute oximetry. Few
52 studies on choroidal oxygenation have been reported and those that have are restricted mainly
53 to animal studies [12]. Due to the close coupling between cerebral and choroidal vasculature,
54 measurement of choroidal oxygenation would provide a surrogate measure of oxygen
55 saturation of the cerebral vasculature. In terms of retinal diseases, choroidal oximetry could
56 prove to be useful in understanding pathophysiology of diseases like age-related macular
57 degeneration [13, 14], diabetic retinopathy [15-17] and be employed as a useful diagnostic tool
58 for Alzheimer's disease risk [18, 19] in which cerebral blood flow plays an important role.

59 The first non-invasive measurement of choroidal oxygen saturation was demonstrated by
60 Broadfoot et al [20] in 1961, using a modified Gullstrand ophthalmoscope to focus light
61 reflected from the human ocular fundus onto a photomultiplier. Light was time-sequentially

1
2
3 62 spectrally filtered using a filter wheel with red and cyan colour filters. The study reported that
4
5 63 the fundus reflection of red light changed significantly when the choroidal oxygenation was
6
7 64 altered in subjects breathing nitrogen or by apnea. Laing et al employed non-imaging fundus
8
9 65 reflectometry at wavelengths of 650 nm and 805 nm to determine the oxygen saturation in the
10
11 66 choroidal blood [21] for subjects with acute mild hypoxia induced by breathing a hypoxic-air
12
13 67 mixture. More recently, Kristjandottir et al [22] imaged oxygen saturation in choroidal vessels
14
15 68 based on images recorded at wavelengths of 570 nm and 600 nm using a modified fundus
16
17 69 camera. The study was however, restricted to subjects with very low pigmentation that
18
19 70 provided sufficient visibility of the choroidal vessels within the retinal images and at the visible
20
21 71 wavelengths suitable for vascular oximetry. Fundus reflection has also been used to quantify
22
23 72 retinal pigments, including macular pigment [23] and melanin [24, 25] as well as to study
24
25 73 diseases and treatment efficacy; for example, in diabetes [26] and glaucoma [27, 28]. A review
26
27 74 of fundus reflection characterisation and its application is presented in [29]. We report here a
28
29 75 proof-of-concept demonstration of a new technique for remote assessment of SpO₂ based upon
30
31 76 reflection of light from the pupil. This is the ‘red-eye’ effect familiar from routine flash-
32
33 77 illuminated photography of faces. It offers oximetry without contact, and in principle at
34
35 78 considerable range, that could be applied, for example, for remote triage in emergency care or
36
37 79 where conventional pulse oximetry is not possible. The red-eye effect is due to light that has
38
39 80 been transmitted into the pupil, and undergoes a two-way transmission through the retinal and
40
41 81 choroidal tissue and is reflected by the sclera at the back of the eye.

42
43 82 The aim of this proof of concept study was to demonstrate the feasibility of remote sensing of
44
45 83 choroidal oxygenation using spectral images of the pupil reflection. We accomplished this by
46
47 84 calculation of spectral optical density ratios of pupil reflections under conditions of normoxia
48
49 85 and during a period of inhaling a hypoxic gas mixture. We hypothesised that the changes in
50
51
52
53
54
55
56
57
58
59
60

1
2
3 86 optical density ratio, as a function of normoxia and hypoxia, would mirror the simultaneously
4
5 87 measured changes in systemic oxygenation determined from finger pulse oximetry.
6
7

8 88 **2. Methods**

9
10
11 89 *2.1 Physical principles of oximetry using pupil red-eye reflection:* In the absence of
12
13
14 90 illumination, the eye pupil appears dark, but with bright illumination from a source located
15
16 91 close to the point of observation, as is common in flash photography, pupils appear red due to
17
18 92 the interaction of light with blood in the ocular fundus. At wavelengths in the region 500-
19
20 93 600nm this reflection is due mainly to bulk optical scattering and reflection from within the
21
22 94 retina. At wavelengths between 630 and 800nm, where the optical transmission of blood is
23
24 95 much higher, a significant fraction of light is transmitted through the retina and choroid and is
25
26 96 reflected by the sclera. At these longer wavelengths, it is the spectral variation in the absorption
27
28 97 of light by choroidal blood that dominates the spectrum of the red-eye reflection: the absorption
29
30 98 by the photoreceptor layer and nerve-fibre layers in the retina is typically less than about 2%
31
32 99 at these wavelengths [30] and does not have a significant impact on our measurements. There
33
34
35 100 is however absorption of light by melanin in the pigment epithelium layer and within the
36
37 101 choroids, which correlates with eye and skin pigmentation of the subject and does affect
38
39 102 measured optical densities.
40
41
42
43

44
45 103 The choroid has an extremely dense vasculature and at about 400 μm thick is much thicker
46
47 104 than the retina and therefore is the dominant determinant to the spectrum of the pupil reflection
48
49 105 in the 630-800 nm range. The technique presented here exploits the spectral variation in the
50
51 106 absorbance coefficients of oxyhaemoglobin and deoxyhaemoglobin; that is, the same principle
52
53 107 on which retinal oximetry is based. The spectrum of light reflected from the choroid is
54
55 108 dependent upon blood-oxygen saturation and the relevant fractions of oxy- and
56
57 109 deoxyhaemoglobin. As for two-wavelength retinal oximetry, using one isosbestic wavelength
58
59
60

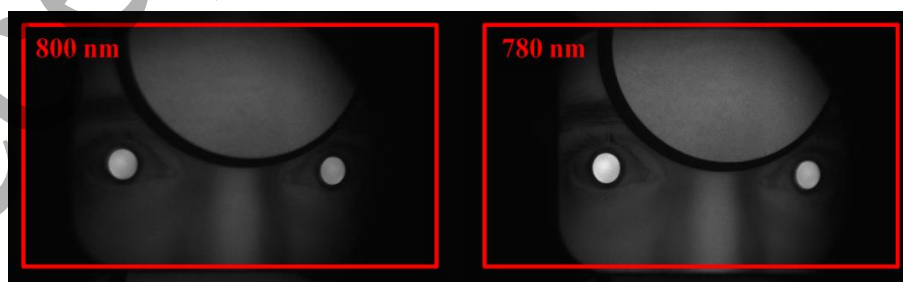
1
2
3 110 and one oxygen-sensitive wavelength to record choroidal reflection, the oxygen saturation of
4
5 111 choroidal blood can be characterised.

6
7
8 112 The geometry for imaging and illumination of the eye and the gaze angle determine the
9
10 113 characteristics of the brightness and spectrum of the fundus reflection. In conventional
11
12 114 photography of faces, red-eye fundus reflection is avoided (for aesthetic reasons) by
13
14 115 displacement of the flash illumination from the camera lens so that the area of the retina
15
16 116 illuminated by the flash lamp has zero or reduced overlap with the area of the retina that is
17
18 117 geometrically visible from the position of the camera lens. We have employed a conventional
19
20 118 fundus camera for which the illumination and imaging optics are coaxial leading to a high
21
22 119 degree of overlap between the illuminated and visible areas of the fundus so as to enhance the
23
24 120 intensity of light returned through the pupil.

25
26
27
28
29
30 121 For spectral imaging of the oximetric fundus reflection, the fundus-camera was moved from
31
32 122 its usual position for imaging through the pupil; with the objective lens about 40 mm from the
33
34 123 eye; to a new position of 90 mm away so as to increase the field of view and enable
35
36 124 simultaneous snapshot spectral imaging of both pupils as can be seen from the images in Figure
37
38
39 125 1.

40
41
42 126 The illumination and image formation is illustrated by the optical ray-trace shown in the upper
43
44 127 image in Figure 2. This was calculated using the *Zemax*© optical design programme and
45
46 128 employing a schematic model for the human eye as reported in [31]. As is conventional for a
47
48 129 mydriatic fundus camera the light is focused to an annulus with an external diameter of 6 mm
49
50 130 located 40 mm from the front objective lens. During conventional imaging of the retina, this
51
52 131 annulus is positioned within the pupil and a glare-free image of the retina is recorded through
53
54 132 the dark non-illuminated centre of the annulus. The emmetropic eye is naturally focused at
55
56 133 infinity (mydriasis is used in our experiments) and so the image plane of the illumination
57
58
59
60

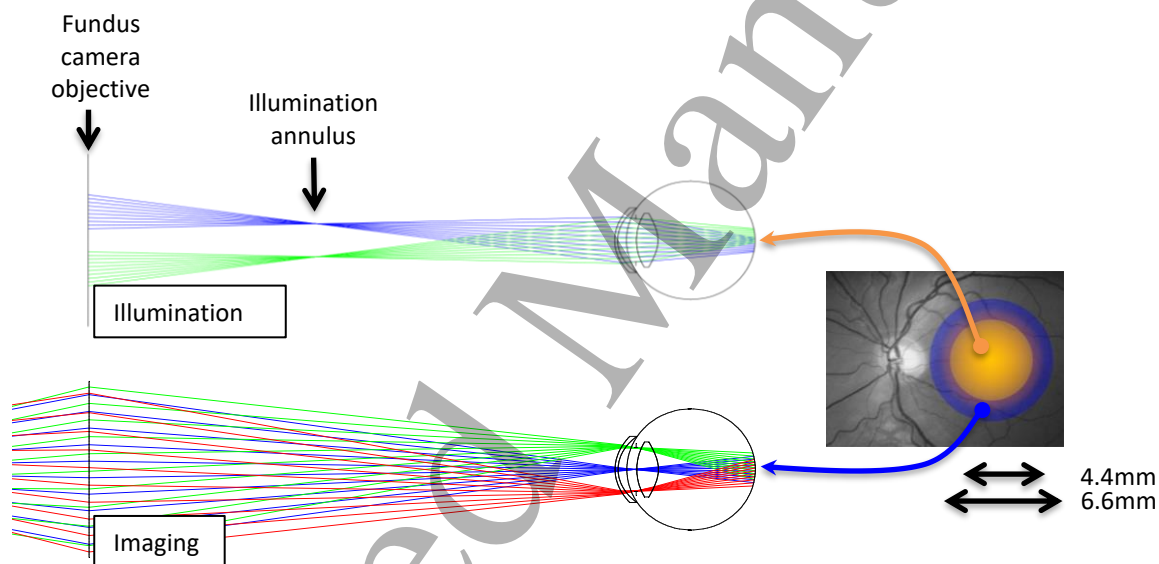
1
2
3 134 annulus is about 10 mm behind the retina and a blurred image of the annulus is formed at the
4
5 135 retina. From the ray-traced model, we determined that the blurred image of the illumination
6
7 136 annulus has a diameter of 4.4 mm at the retina, however lateral diffusion of light results in a
8
9 137 significantly wider disk being illuminated. We employed ray tracing to simulate how
10
11 138 illumination by the retinal illumination affects the image formed of the pupil by the retinal
12
13 139 camera. This showed that a disc of 6.6 mm at the retina contributes to the imaged pupil
14
15 140 radiance, which we call the imaged-pupil radiance (IPR) disc. The approximate relative
16
17 141 dimensions of the illumination and IPR discs are depicted by the orange and blue discs
18
19 142 superimposed on a typical retinal image in Figure 2. At these infrared wavelengths, the tissue
20
21 143 point-spread function of the retina is quite large, between 1-2 mm, effectively blurring and
22
23 144 expanding the illumination disc on the retina to fill the IPR disc. It is apparent from Figure 2
24
25 145 that the pupil radiance image is determined by the integral of the light scattered from within
26
27 146 the IPR disc and will therefore be expected to vary homogeneously across the pupil, but will be
28
29 147 increased when the optic disc (which has a high albedo) falls within the IPR disc leading to
30
31 148 localised brightness spots within the pupil image. Thus, when the subject fixates on the
32
33 149 illumination point, the IPR disc is centred on the macula and the image of the pupil is
34
35 150 determined by two-way transmission of light through the macula and surrounding retina,
36
37 151 through the choroid to the sclera, enabling high-quality choroidal oximetry. If the direction of
38
39 152 gaze is turned nasally however, the optic disc reflection contributes to the IPR disc
40
41 153 contaminating the pupil image with scattered light and has the reduced interaction with the
42
43 154 choroid.
44
45
46
47
48
49
50
51
52



1
2
3 **Figure 1.** A spectral image of the upper face captured by IRIS system. The two pupil reflexes are visible together
4 with a calibration tile. The two sub-images used for choroidal oximetry were 800 nm as isosbestic and 780 nm as
5 oxygen sensitive are shown above.
6
7
8
9

159

10 To determine whether, for typical measurements, the optic disc intrudes into the IPR disc and
11 contaminates the pupil images, the effect of the angle of gaze on fundus reflection was
12 determined by recording fundus-reflection pupil images for two subjects as the angle of gaze
13 was changed from an extreme nasal side to extreme temporal side as the subject tracked the
14 fundus-camera fixation light. The fundus ODR was calculated for five images at each angle of
15 gaze. The effect of angle of gaze on ODR is presented in section 3.1.
16
17
18
19
20
21
22
23
24
25
26
27
28
29
30
31
32
33
34
35
36
37
38
39
40
41
42
43
44
45

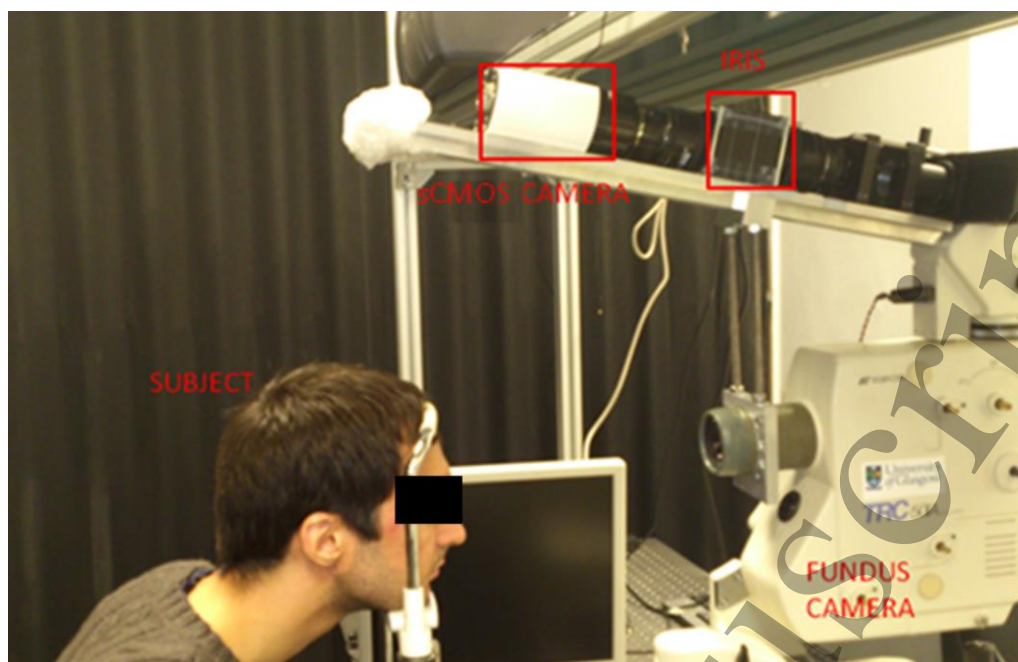


166

46 **Figure 2.** Optical ray-trace of the illumination of the retina by the fundus camera for an emmetropic eye (upper
47 ray trace) and of the fundus contributing to the radiance imaged at the pupil (lower ray trace). The inset image
48 depicts the illumination (blue) and reflex (orange) discs superimposed on an image of a typical retina and centred
49 on the macula.
50

51 **2.2 Imaging Setup:** Spectral images were acquired using a modified commercial fundus camera
52 (Topcon TRC 50 IA, Japan) fitted with an image-replicating imaging spectrometer (IRIS), (see
53 Figure 3), which acquires images in a single snapshot at eight wavelengths optimised for
54 oximetry [32-36], IRIS consists of a cascade of two-beam polarising interferometers that
55 simultaneously spectrally filter and replicate images to yield, in this case, eight narrowband
56
57
58
59
60

1
2
3 176 images onto a single detector array. Interferometric spectral filtering by IRIS provides the well-
4
5 177 known Fellgett multiplex advantage of two-beam interferometry [37] enabling the highest
6
7 178 possible signal-to-noise ratios to be attained with the limited optical intensities that can be
8
9 179 safely used with the eye. We employed an IRIS system for which the waveplates had been
10
11 180 optimised for retinal vascular oximetry, providing isosbestic and oxygen-sensitive spectral
12
13 181 bands in the region 560-605 nm. Because IRIS passbands spectrally replicate with a specific
14
15 182 free-spectral range in a manner similar to a Fabry-Perot interferometer, it has thus been possible
16
17 183 to use this IRIS design for spectral imaging in the near infrared simply by the use of a different
18
19 184 spectral bandpass filter to restrict the free spectral range to a region in the near infrared. We
20
21 185 employed a 25 nm bandwidth band-pass filter with centre wavelength 788 nm to spectrally
22
23 186 filter light from the fundus camera inspection lamp, restricting the measurement to the free-
24
25 187 spectral range of IRIS for which only a single spectral transmission lobe occurs. The spectral
26
27 188 transmission functions of the eight sub-images of this IRIS system in the wavelength range
28
29 189 760-850 nm are shown in Figure 3. From the eight spectrally filtered images, two images with
30
31 190 spectral transmission peaks at 780 nm and 800 nm were employed to calculate optical density
32
33 191 ratio. The image at 780 nm provides sensitivity to blood oxygenation and 800 nm corresponds
34
35 192 to an isosbestic wavelength for which absorbance is approximately independent of
36
37 193 oxygenation.
38
39
40
41
42
43
44
45
46
47
48
49
50
51
52
53
54
55
56
57
58
59
60



194

195 **Figure 3:** Experimental setup of the modified fundus camera to record the red eye pupil reflection.

196 The objective of the fundus camera was located 90 ± 5 mm away from the eyes of the subjects
197 with the head stabilised using a headrest. The eyes of the subjects were illuminated with the
198 filtered infra-red light and the spectral images of the pupils were captured simultaneously by a
199 sCMOS camera (Zyla, Andor; Belfast, U.K.) located to intercept the image relayed through
200 IRIS from the image plane of the fundus camera. An example of a captured raw image is shown
201 in Figure 1.

202

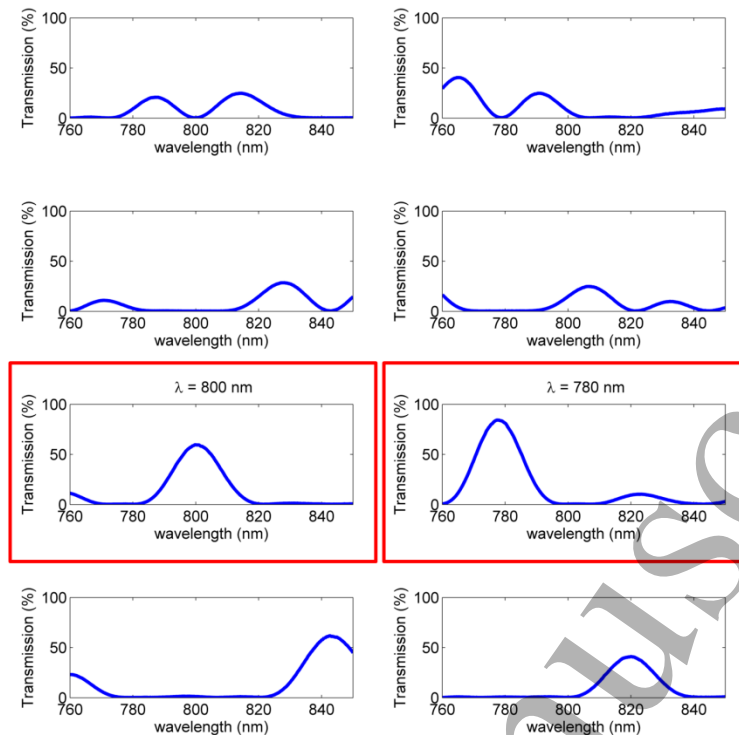


Figure 4. Spectral transmissions of 8 sub-images recorded with the IRIS imaging system. The two sub-images used for choroidal optical density ratio measurements were 800 nm and 780 nm and are highlighted in red.

2.3. Oximetric analysis:

We assume that optical attenuation of infrared light transmitted through the choroid obeys the Beer-Lambert law and therefore, as described in the appendix, the ratio of the optical densities for light transmission recorded at oxygen-sensitive and isosbestic wavelengths varies in proportion to blood oxygenation as has been demonstrated by Beach et al [38] for oximetry of the retinal vasculature. For application in the retina, the optical density of the vasculature is determined by the ratio of intensity at the centre of a blood vessel to an estimate of the reflected light in the absence of the vessel determined by interpolation of the light on either side of the vessel. In an analogous metric, we define the optical density ratio as

$$ODR = \frac{\log_{10} R^{780}}{\log_{10} R^{800}} = \frac{\log_{10} \frac{v_p^{780}}{v_c^{780}}}{\log_{10} \frac{v_p^{800}}{v_c^{800}}} \quad (1.0)$$

1
2
3
4 217 Where, $R^\lambda = \frac{v_p^\lambda}{v_c^\lambda}$ is the ratio of the average intensities of the images of the pupil and a
5
6
7 218 calibration tile (visible in front of the forehead in Figure 1) at wavelengths $\lambda = 780$ nm and 800
8
9 219 nm. In the appendix we show that the ODR varies linearly with oxygen saturation of choroidal
10
11 220 blood. At 780 nm blood becomes increasingly transparent with increasing oxygenation causing
12
13 221 the ODR to increase. Note that the light emitted by the pupil is non-Lambertian, concentrating
14
15 222 light towards the source and transmission, and the absorbance of the choroid is low. So the
16
17 223 pupil image can be brighter than a unity-albedo reflector. Although both pupils can be imaged
18
19 224 simultaneously, the results presented here are based on one pupil (right).

225 2.4. Fundus ODR with Changing Inspired Oxygen in Healthy Human Subjects

226 Ten healthy subjects were recruited to this study (eight males and two females, age 27 ± 9 years
227 mean \pm SD;). Written informed consent was obtained from all subjects. Subjects were briefed
228 about the experimental procedure and asked to refrain from consuming any alcohol or
229 caffeinated drink on the day prior to the experiment. The study was approved by the Heriot-
230 Watt University Ethics Committee. All procedures were performed in accordance with the
231 tenets of the Declaration of Helsinki. All the subjects recruited were healthy, non-smokers,
232 without history of a respiratory disorder and taking no medication.

233 On the day of study, they were again briefed about the experimental protocol. Age, sex, weight
234 was recorded. Tropicamide (1%, Bausch & Lomb, Chauvin Pharmaceuticals, Ltd., U.K.) was
235 used to dilate the pupil. After about ten to fifteen minutes maximum dilation of the pupils,
236 typically 8 mm, was achieved and the subjects were ready to be imaged.

237 Pupil reflection images were acquired for all the subjects under normoxia (21 % inspired
238 oxygen). Hypoxia was then induced by changing the inspired oxygen to 15 % using a hypoxia
239 generator (Everest Summit II Hypoxic Generator; Hypoxico, Inc., New York, NY, USA). [39]

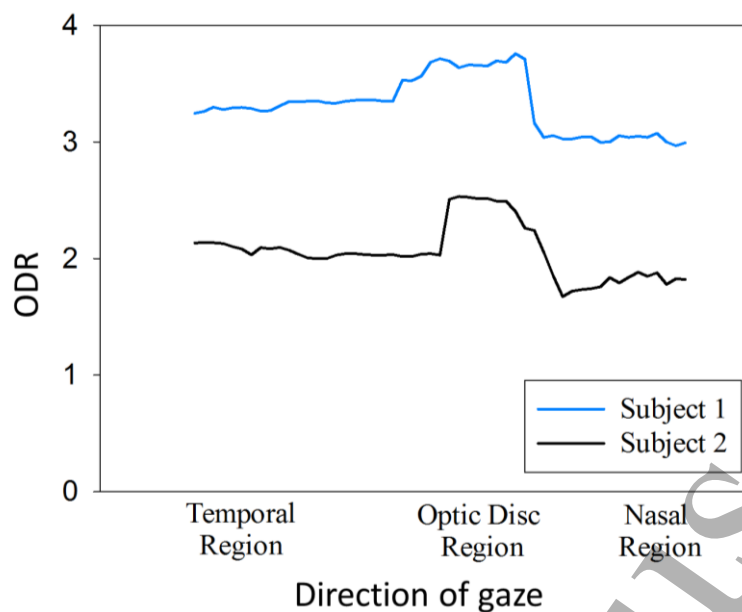
240 Pupil reflection images were acquired under hypoxic conditions. In total five sets of images

1
2
3 241 were acquired- three under normoxia and two under hypoxia (in alternating order). The
4
5 242 peripheral arterial oxygen saturation was monitored using fingertip pulse oximeter
6
7 243 (AUTOCORR; Smiths Medical ASD Inc., Rockland, MA, USA) during both normoxia and
8
9 244 hypoxia conditions. All images (normoxic and hypoxic conditions) were analysed to calculate
10
11 245 the fundus ODR. A paired t-test (SigmaPlot, Systat Software Inc.) was used to determine
12
13 246 significance of the result.
14
15
16
17

18 247 **3. Results**

21 248 *3.1. Effect of Angle of Gaze on Fundus ODR*

23 249 As previously discussed, it was assumed that when the subject fixates on a compact light source
24
25 250 imaged on the macula, only the choroid and retina will contribute to the fundus reflection, but
26
27 251 that some misalignment of the gaze may introduce a contribution from the optic disc and that
28
29 252 this would modify the oximetric spectral signature. To assess this potential issue the effect of
30
31 253 the angle of gaze on the pupil image was analysed in two subjects. Figure 5 shows the effect
32
33 254 of the angle of gaze on the ODR for two subjects as the angle of gaze was changed from extreme
34
35 255 temporal through to extreme nasal. The change in gaze direction corresponds to sweeping the
36
37 256 area of the fundus contributing to the pupil image from the temporal fundus, macular region,
38
39 257 optic disc to nasal side of the fundus. The elevated plateau in the ODR corresponds to angle
40
41 258 for which the reflection from the optic disc contributes and hence for which the pupil image is
42
43 259 both brighter and whiter. The gaze angles for which the optic-disc reflection partially
44
45 260 contributes to the pupil image is apparent from the presence of brighter areas in a non-uniform
46
47 261 pupil image and are thus easily identified and avoided.
48
49
50
51
52
53
54
55
56
57
58
59
60



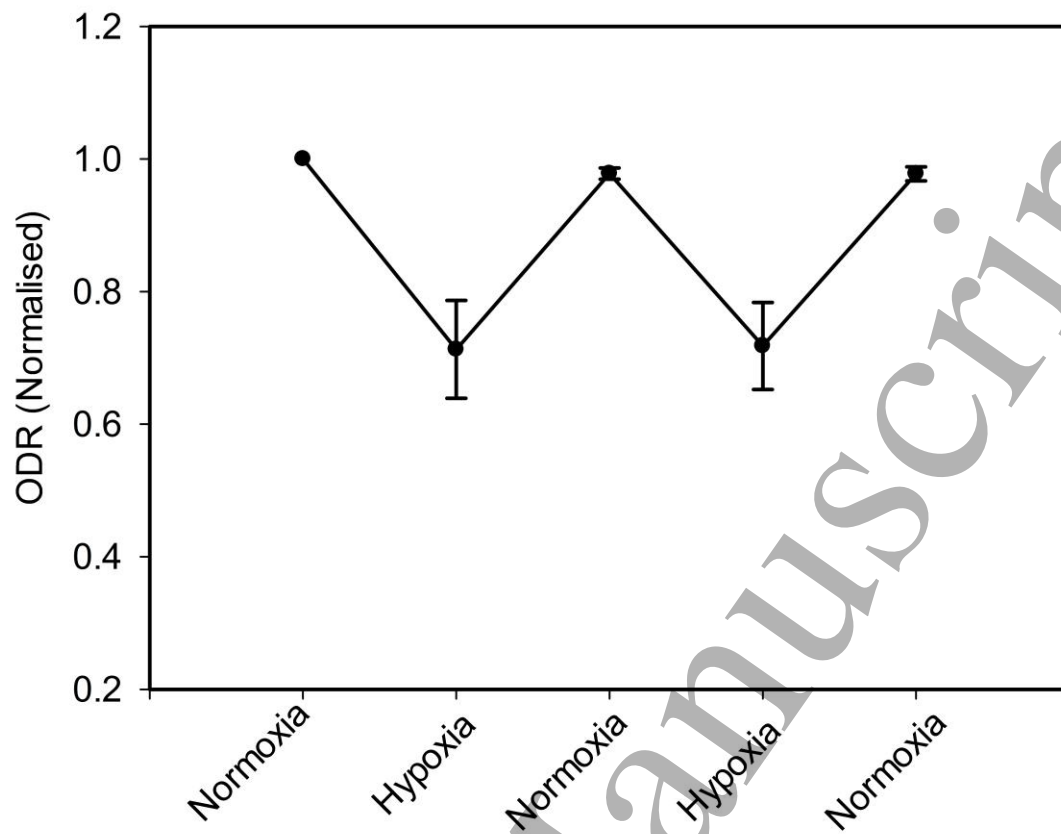
262

263 **Figure 5.** Variation of pupil image ODR with the angle of gaze. The high ODR plateau region corresponds to
 264 the optic disc which is closer to white than the rest of the fundus.

265

266 3.2. Fundus ODR with Change in Inspired Oxygen in Healthy Human Subjects

267 The variation in ODR was determined as the inspired gas was cycled between normoxic 21 %
 268 (Fraction of Inspired oxygen) FiO_2 , and hypoxic 15 % FiO_2 conditions. A pulse oximeter
 269 (AUTOCORR; Smiths Medical ASD Inc., Rockland, MA, USA) placed over the index finger
 270 throughout the experiment monitored and recorded oxygen saturation. The recorded variation
 271 in ODR (normalised with the first normoxia measurements), averaged over 2.5
 272 normoxic/hypoxic cycles, is shown for ten subjects in Figure 6 and the variation in average
 273 ODR with pulse oximetry is shown in Figure 7. The reduction in ODR between each level of
 274 normoxic and hypoxic FiO_2 and also with fingertip pulse oximetry is highly significant ($P <$
 275 0.001 for each case).



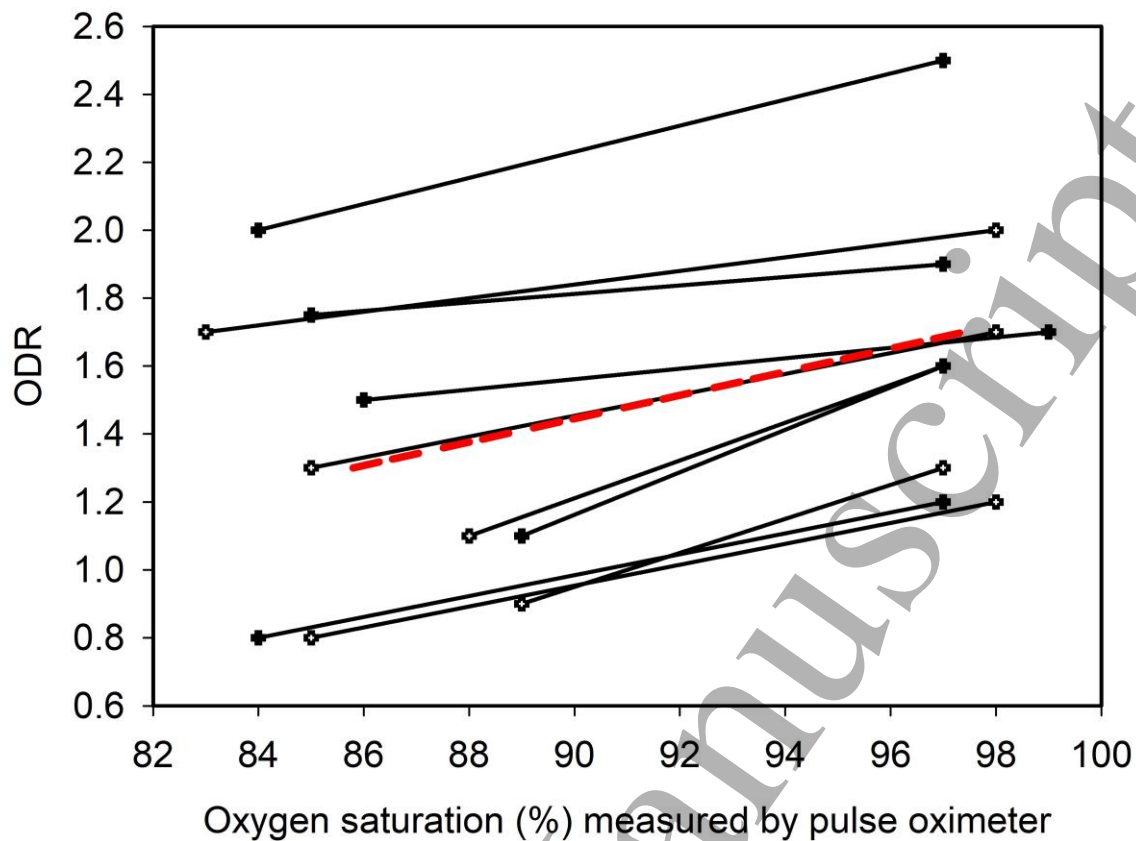
276

277 **Figure 6.** Changes in optical density ratio (normalised) as a function of either normoxia (21 % FiO₂, O₂ Saturation
278 97 %) or hypoxia (15 % FiO₂, O₂ Saturation 86 %) in ten subjects. ODR was found to be directly proportional to
279 pulse oxygen saturation.

280

281

282



283

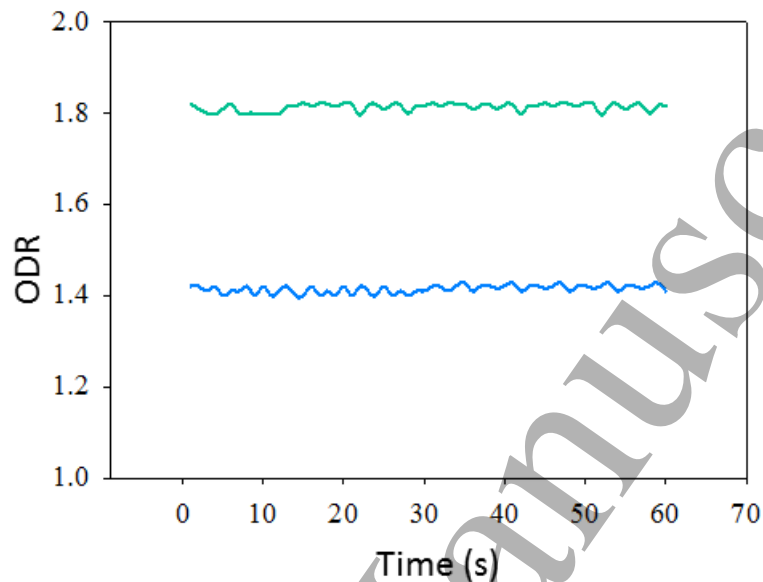
284 **Figure 7.** Oxygen saturation measured by pulse oximeter versus changes in optical density ratio in each of the
 285 ten subjects. Each black line represents one of the subjects and the red dotted line is averaged ODR of the ten
 286 subjects at hypoxia and normoxia.

287 The repeatability and stability of the technique was demonstrated by the temporal recordings
 288 of ODR for two subjects over a period of 60 seconds when breathing room air as shown in
 289 Figure 8, showing a root-mean-square variation of 0.019 compared to a typical modulation in
 290 ODR of 0.3: a signal-to-noise ratio of 16. The average gradient of the variation of ODR with
 291 oxygenation saturation is 3.47 and so the noise-like variations in Figure 8 correspond to noise-
 292 equivalent variations in oxygen saturation of 0.5%.

293 Collectively, the data in Figures 6, 7 and 8, illustrates that the decrease in ODR mirrored the
 294 effect of changing the inspired gas mixture. Measurement of choroidal ODR enabled sensing
 295 of a reduction in systemic blood oxygenation during hypoxia exposure. This observation was

296 supported by the pulse oximeter data and the fact that the ODR remained stable over time (60
297 seconds).

298



299

300 **Figure 8.** Pupil Optical Density Ratio for two subjects, (as indicated by green and blue lines) at room air with
301 respect to time.

302 **4. Discussion**

303 In this study, a non-invasive method to sense oxygen saturation in choroidal blood is presented.

304 The pupil ODR is sensitive to blood oxygenation and declines with a decrease in blood
305 oxygenation, as demonstrated in human subjects breathing gas with a reduced oxygen content.

306 The pupil ODR was assessed under normoxia in healthy human subjects and was found to
307 decrease significantly ($P < 0.001$) when compared with the hypoxia condition. At both
308 normoxia and hypoxia arterial blood-oxygen saturation was monitored with a finger-tip pulse
309 oximeter. The pupil reflection was recorded simultaneously for three normoxia stages and two
310 hypoxia stages for each subject. The fundus ODR decreased significantly between each stage

1
2
3 311 of normoxia and hypoxia (Figure 5) for all the ten subjects. The fundus ODR was also recorded
4
5 312 for 60 seconds at room air for two subjects, and was found to be stable with time (Figure 8).
6
7

8 313 The results presented in this study are comparable with the results obtained by Broadfoot[20]
9
10 314 and by Laing[21]: both studies reported a decrease in the reflection intensity with a decrease in
11
12 315 blood oxygenation. The imaging and recording setup presented here, however, is simpler and
13
14 316 has advantages over the methods used in those two previous studies [20, 21]. In their
15
16 317 experimental methodology, the imaging system comprised of a fundus camera to image the
17
18 318 eye, and an elaborate electronic system with photomultipliers and photodiodes to record the
19
20 319 intensity of the reflections from the eye. Broadfoot used a filter wheel assembly to time-
21
22 320 sequentially record the intensity at different wavelengths whereas Laing's apparatus used
23
24 321 dichroic mirrors to separate reflections at two wavelengths, which were recorded
25
26 322 simultaneously with two photodiodes. The setup presented here has a fundus camera fitted with
27
28 323 an IRIS device, which enables recording of spectral images at multiple wavelengths in a single
29
30 324 snapshot onto a single detector. The advantage of using snapshot imaging ensures that pupil
31
32 325 images at different wavelengths were captured at the same point of time thus removing any
33
34 326 variability due to a temporal difference in recordings. Our device recorded the spectral images
35
36 327 and the ODR was subsequently calculated from the images. Any eye movement was then
37
38 328 easily corrected by image registration to enable a time-series measurement of choroidal
39
40 329 oxygenation. Any faulty image frame or eye-blinks could also be easily identified and removed
41
42 330 from the data. Previous protocols [20, 21] that have used the reflection intensity, which was
43
44 331 directly recorded onto a photodiode with the corrections employed in the present study, would
45
46 332 not have been possible. The other advantage of the technique presented here is that it can be
47
48 333 used to image both eyes simultaneously, although the data presented in figures 5, 6 and 7 are
49
50 334 based on images from one pupil only.
51
52
53
54
55
56
57
58
59
60

1
2
3 335 While increased oxygen tension has considerable constrictive effect on retinal vessels, such
4
5 336 effect is minor in the choroid. The morphological effect of oxygen tension on the choroid is
6
7 337 minimal to none and choroidal vasoconstriction unlikely to influence OD. Previous studies on
8
9 338 choroidal and retinal oxygen saturation using the Oxymap T1 device support this [22].
10
11
12

13 339 While using the fundus ODR for calculating oxygen saturation, it is important to know which
14
15 340 region of the fundus (and underlying choroid) is being sampled. The process depends mainly
16
17 341 on the direction of gaze as described earlier in section 3.1. The effect of direction of the gaze
18
19 342 on fundus ODR was also assessed (Figure 4). It is important that when using fundus reflections
20
21 343 for oximetry purposes, to sample a constant region of the fundus and to avoid imaging the optic
22
23 344 disc. Consequently, only the macula region was illuminated during pupil reflection
24
25 345 experiments. Furthermore the avascular nature of the macular region means the sampled region
26
27 346 is dominated by choroidal blood.
28
29
30
31

32 347 In this study, we have demonstrated proof-of-principle recording in dark conditions. Future
33
34 348 work will refine the technique for use in ambient light by employing calibration and correction
35
36 349 of the reflection of ambient light from a calibration surface and the use of alternatives to a
37
38 350 calibration tile for calibration – for example, the sclera can also serve as an approximate
39
40 351 calibration. Reflection of ambient light from the retina is negligible compared to the reflection
41
42 352 of the flash illumination and can be neglected.
43
44
45
46

47 353 We have successfully demonstrated in human subjects that fundus ODR is capable of detecting
48
49 354 changes in blood oxygenation and that these measures correspond to changes observed using
50
51 355 pulse oximetry suggesting that the ODR can be used to calculate choroidal oxygenation. For
52
53 356 all the subjects, ODR decreased from an average value of $1.7 (\pm 0.4)$ to $1.3 (\pm 0.4)$ during the
54
55 357 period of inhaling the hypoxic gas mixture which tracked the changes in pulse oximeter values
56
57
58 358 from $97 (\pm 0.5) \%$ to $86 (\pm 2) \%$. Thus we have demonstrated the ability to measure intra-
59
60

1
2
3 359 subject changes in blood oxygenation, the large inter-subject variability is due to differences
4
5 360 in retinal pigment epithelial layer between subjects. These differences indicate that for absolute
6
7 361 oximetry a process of calibration would be required for each subject. Future work should aim
8
9
10 362 to understand and reduce this inter-subject variability. One way to characterise the fundus and
11
12 363 choroidal pigmentation could be to record the iris and skin colour and estimate the choroidal
13
14 364 pigmentation based on these characteristics [40].
15
16

17
18 365 The results described in this study were based on a small number of subjects ($n = 10$). A study
19
20 366 based on a larger number of subjects that comprises individuals with a range of iris and skin
21
22 367 colour would be useful to determine the degree of variability across a more general population.
23
24

25 368 There are certain advantages from using fundus reflection oximetry over retinal oximetry. A
26
27 369 good quality retinal image is crucial to perform retinal oximetry which requires proper imaging
28
29 370 technique and training. In contrast, fundus reflection images are relatively easy to acquire.
30
31 371 Retinal oximetry image analysis is a lengthy and complex process when compared to fundus
32
33 372 reflection oximetry. The other unique advantage is that unlike retinal oximetry, fundus
34
35 373 reflection oximetry could be performed in both the eyes simultaneously.
36
37
38
39

40 374 The method we present involves co-axial illumination and spectral imaging of pupils,
41
42 375 exploiting the spectral signature applied to light emitted from the pupil following two-way
43
44 376 transmission through the choroid. Although it is similar to the work of Broadfoot et al[20] and
45
46 377 Laing et al[21], these researchers employed techniques that are essentially non imaging and
47
48 378 time sequential; they utilised modified ophthalmoscopes to focus light reflected from the
49
50 379 fundus, through the pupil onto single photodetectors. In contrast, we have imaged the pupil to
51
52 380 record the light reflected by the ocular fundi at multiple wavelengths in a single snapshot. This
53
54 381 apparatus has enabled remote (~ 90 mm standoff) assessment of choroidal oxygenation and
55
56 382 demonstrates that, in principle; oximetry at large standoff ranges is also possible. The technique
57
58
59
60

1
2
3 383 has possible applications for remote triage in emergency medicine or systemic blood oximetry
4
5 384 in for example sport or high-stress activities or in scenarios where pulse oximeter is limited
6
7 385 e.g. motion artefacts, low pulse problem, pigmentation, and poor perfusion (due to cold, shock,
8
9 386 sepsis or heart attack). Furthermore, this technique could be adapted for simultaneous imaging
10
11 387 of both eyes which opens the possibility of temporally-resolved bilateral discrimination of
12
13 388 ocular disparity and systemic oximetry effects.
14
15

16
17 389 Measurement of Choroidal-oxygen saturation could provide a viable surrogate measurement
18
19 390 of oxygen saturation in the cerebral vasculature. Such an approach could be useful in
20
21 391 understanding the pathophysiology of diseases such as age-related macular degeneration[13,
22
23 392 14], diabetic retinopathy[15, 16] in which choroidal blood flow plays an important role [22].
24
25 393 Other potential application includes blood loss and internal bleeding assessment in trauma
26
27 394 victims. Using this technique, we may also detect arrival of a de-saturation signal from the
28
29 395 lungs to the blood circulation of both the eyes, a technique that could potentially be useful in
30
31 396 detecting carotid artery stenosis.
32
33
34
35

36
37 397 In conclusion, the particular advantage of the technique presented in this pilot study on ten
38
39 398 healthy individuals is the standoff sensing of the oxygenation of blood in the choroidal
40
41 399 circulation as a proxy for systemic and cerebral oxygenation. We have demonstrated a
42
43 400 measurement precision of 0.5% for short-term changes in blood oxygenation. We have
44
45 401 employed relatively high-cost laboratory equipment that was available to us, however the
46
47 402 technique could be readily implemented using low cost mass-produced cameras and, for
48
49 403 example, LED illumination.
50
51
52

53 404 **Acknowledgement**

54
55
56
57 405 The author's have confirmed that any identifiable participants in this study have given their
58
59 406 consent for publication.
60

407 **References**

- 408 1. Wise, G.N., C.T. Dollery, and P. Henkind, *The retinal circulation*. 1971, New York: Harper &
- 409 Row.
- 410 2. Birol, G., et al., *Oxygen distribution and consumption in the macaque retina*. American Journal
- 411 of Physiology - Heart and Circulatory Physiology, 2007. **293**(3): p. H1696-H1704.
- 412 3. Tachibana, H., F. Gotoh, and Y. Ishikawa, *Retinal vascular autoregulation in normal subjects*.
- 413 *Stroke*, 1982. **13**(2): p. 149-55.
- 414 4. Alm, A. and A. Bill, *Blood Flow and Oxygen Extraction in the Cat Uvea at Normal and High*
- 415 *Intraocular Pressures*. Acta Physiologica Scandinavica, 1970. **80**(1): p. 19-28.
- 416 5. Hardarson, S.H., et al., *Automatic Retinal Oximetry*. Investigative Ophthalmology & Visual
- 417 Science, 2006. **47**(11): p. 5011-5016.
- 418 6. Hammer, M., et al., *Retinal vessel oximetry-calibration, compensation for vessel diameter and*
- 419 *fundus pigmentation, and reproducibility*. Journal of Biomedical Optics, 2008. **13**(5): p.
- 420 054015-054015-7.
- 421 7. Beach, J.M., et al., *Oximetry of retinal vessels by dual-wavelength imaging: calibration and*
- 422 *influence of pigmentation*. Journal of Applied Physiology, 1999. **86**(2): p. 748-758.
- 423 8. Choudhary, T.R., et al., *Assessment of Acute Mild Hypoxia on Retinal Oxygen Saturation Using*
- 424 *Snapshot Retinal Oximetry*. Investigative Ophthalmology & Visual Science, 2013. **54**(12): p.
- 425 7538-7543.
- 426 9. Blumenroder, S., A.J. Augustin, and F.H. Koch, *The influence of intraocular pressure and*
- 427 *systemic oxygen tension on the intravascular pO₂ of the pig retina as measured with*
- 428 *phosphorescence imaging*. Surv Ophthalmol, 1997. **42 Suppl 1**: p. S118-26.
- 429 10. Wilson, D.F., et al., *Oxygen distribution and vascular injury in the mouse eye measured by*
- 430 *phosphorescence-lifetime imaging*. Applied optics, 2005. **44**(25): p. 5239-5248.
- 431 11. Linsenmeier, R.A., et al., *Retinal hypoxia in long-term diabetic cats*. Invest Ophthalmol Vis Sci,
- 432 1998. **39**(9): p. 1647-57.
- 433 12. Ahmed, J., et al., *Oxygen distribution in the macaque retina*. Investigative Ophthalmology &
- 434 Visual Science, 1993. **34**(3): p. 516-521.
- 435 13. Pournaras, C.J., et al., *Regulation of Subfoveal Choroidal Blood Flow in Age-Related Macular*
- 436 *Degeneration*. Investigative Ophthalmology & Visual Science, 2006. **47**(4): p. 1581-1586.
- 437 14. Friedman, E., *A hemodynamic model of the pathogenesis of age-related macular*
- 438 *degeneration*. American journal of ophthalmology, 1997. **124**(5): p. 677-682.
- 439 15. Nagaoka, T., et al., *Alteration of choroidal circulation in the foveal region in patients with type*
- 440 *2 diabetes*. British Journal of Ophthalmology, 2004. **88**(8): p. 1060-1063.
- 441 16. Schocket, L.S., et al., *Foveolar choroidal hemodynamics in proliferative diabetic retinopathy*.
- 442 *International ophthalmology*, 2004. **25**(2): p. 89-94.
- 443 17. Langham, M.E., et al., *Choroidal blood flow in diabetic retinopathy*. Experimental Eye
- 444 Research, 1991. **52**(2): p. 167-173.
- 445 18. Roher, A.E., et al., *Cerebral blood flow in Alzheimer's disease*. Vascular Health and Risk
- 446 Management, 2012. **8**: p. 599-611.
- 447 19. Mazza, M., et al., *Primary cerebral blood flow deficiency and Alzheimer's disease: shadows and*
- 448 *lights*. J Alzheimers Dis, 2011. **23**(3): p. 375-89.
- 449 20. Broadfoot, K.D., J. Gloster, and D.P. Greaves, *Photoelectric method of investigating the*
- 450 *amount and oxygenation of blood in the fundus oculi*. British Journal of Ophthalmology, 1961.
- 451 **45**(3): p. 161-182.
- 452 21. Laing, R.A., L.A. Danisch, and L.R. Young, *The choroidal eye oximeter: an instrument for*
- 453 *measuring oxygen saturation of choroidal blood in vivo*. Biomedical Engineering, IEEE
- 454 Transactions on, 1975(3): p. 183-195.
- 455 22. Kristjansdottir, J.V., et al., *Choroidal Oximetry With a Noninvasive Spectrophotometric*
- 456 *Oximeter*. Investigative Ophthalmology & Visual Science, 2013. **54**(5): p. 3234-3239.

- 1
2
3 457 23. Elsner, A.E., et al., *Reflectometry with a scanning laser ophthalmoscope*. Applied Optics, 1992.
4 458 **31**(19): p. 3697-3710.
- 5 459 24. Hunold, W. and P. Malessa, [*Spectrophotometric determination of melanin pigmentation of*
6 460 *the human fundus oculi*]. Ber Zusammenkunft Dtsch Ophthalmol Ges, 1974. **72**: p. 246-50.
- 7 461 25. Delori, F.C. and K.P. Pflibsen, *Spectral reflectance of the human ocular fundus*. Applied Optics,
8 462 1989. **28**(6): p. 1061-1077.
- 9 463 26. Augsten, R., et al., *Nonproliferative diabetic retinopathy-reflection spectra of the macula*
10 464 *before and after laser photocoagulation*. Ophthalmologica, 1998. **212**(2): p. 105-11.
- 11 465 27. Cooper, R.L., R.H. Eikelboom, and C.J. Barry, *Correlations between densitometry of red-free*
12 466 *photographs and reflectometry with the scanning laser ophthalmoscope in normal subjects*
13 467 *and glaucoma patients*. Int Ophthalmol, 1992. **16**(4-5): p. 243-6.
- 14 468 28. Eikelboom, R.H., R.L. Cooper, and C.J. Barry, *An improved method of densitometry of red-free*
15 469 *retinal nerve fibre layer photographs*. Aust N Z J Ophthalmol, 1993. **21**(4): p. 219-26.
- 16 470 29. Berendschot, T.T., P.J. DeLint, and D. van Norren, *Fundus reflectance--historical and present*
17 471 *ideas*. Prog Retin Eye Res, 2003. **22**(2): p. 171-200.
- 18 472 30. Hammer, M., et al., *Optical properties of ocular fundus tissues--an in vitro study using the*
19 473 *double-integrating-sphere technique and inverse Monte Carlo simulation*. Physics in Medicine
20 474 and Biology, 1995. **40**(6): p. 963-978.
- 21 475 31. Watkins, R. *OpticStudio models of the human eye*. 2013; Available from:
22 476 [https://customers.zemax.com/os/resources/learn/knowledgebase/zemax-models-of-the-](https://customers.zemax.com/os/resources/learn/knowledgebase/zemax-models-of-the-human-eye)
23 477 [human-eye](https://customers.zemax.com/os/resources/learn/knowledgebase/zemax-models-of-the-human-eye).
- 24 478 32. Gorman, A., D.W. Fletcher-Holmes, and A.R. Harvey, *Generalization of the Lyot filter and its*
25 479 *application to snapshot spectral imaging*. Optics Express, 2010. **18**(6): p. 5602-5608.
- 26 480 33. Alabboud, I., et al., *New spectral imaging techniques for blood oximetry in the retina*. Proc.
27 481 SPIE 6631, Novel Optical Instrumentation for Biomedical Applications III., 2007: p. 66310L-
28 482 66310L.
- 29 483 34. Mordant, D.J., et al., *Spectral imaging of the retina*. Eye, 2011. **25**(3): p. 309-320.
- 30 484 35. Mordant, D.J., et al., *Validation of human whole blood oximetry, using a hyperspectral fundus*
31 485 *camera with a model eye*. Invest Ophthalmol Vis Sci, 2011. **52**(5): p. 2851-9.
- 32 486 36. MacKenzie, L.E., et al., *In vivo oximetry of human bulbar conjunctival and episcleral*
33 487 *microvasculature using snapshot multispectral imaging*. Experimental Eye Research.
- 34 488 37. Harvey, A.R., et al. *Technology options for imaging spectrometry*. 2000.
- 35 489 38. Beach, J.M., et al., *Oximetry of retinal vessels by dual-wavelength imaging: calibration and*
36 490 *influence of pigmentation*. J Appl Physiol (1985), 1999. **86**(2): p. 748-58.
- 37 491 39. Spurling, K.J., C. Zammit, and S. Lozewicz, *Mains-powered hypoxic gas generation: a cost-*
38 492 *effective and safe method to evaluate patients at risk from hypoxia during air travel*. Thorax,
39 493 2011. **66**(8): p. 731-732.
- 40 494 40. Franssen, L., J.E. Coppens, and T.J.T.P. van den Berg, *Grading of Iris Color with an Extended*
41 495 *Photographic Reference Set*. Journal of Optometry, 2008. **1**(1): p. 36-40.

496 Appendix

497 Here we show that there is a linear relationship between the Optical Density Ratio (ODR) and
498 blood oxygen saturation (s). Our fundamental measurement is of the average intensity of light
499 at the detector corresponding to the radiance at the calibration tile and at the pupil at two

1
2
3 500 wavelengths. If we assume the calibration tile to be Lambertian, then the output of a detector
4
5 501 pixel in the image of the tile is given by
6

$$7 \quad 8 \quad 9 \quad 502 \quad v_c = \eta A^\lambda \pi L_0^\lambda N_i^2 \quad (1)$$

10
11
12 503 where A^λ is the albedo of the tile, L_0^λ is the irradiance in the plane of the tile and pupil due to
13
14 504 the light source, N_i is numerical aperture of the entrance aperture of the imaging system and η
15
16 505 is a conversion factor taking into account the responsivity of the detector and the image-space
17
18 506 numerical aperture of the imaging system. The total optical power illuminating the retina
19
20 507 through the pupil is therefore $a_p L_0^\lambda$ where a_p is the area of the pupil. For simplicity, we will
21
22 508 assume that this light is scattered by the sclera with two-way transmission through the choroid
23
24 509 and attenuated according to the Beer-Lambert law. We also assume that the light intensity
25
26 510 illuminating the pupil due to illumination by the retinal reflection is uniform (although we
27
28 511 observe departures from this approximation). To a good approximation the scattering by the
29
30 512 calibration tile is Lambertian and the irradiance at the pupil is independent of the illumination
31
32 513 distribution at the retina and is therefore equal to $a_p L_0^\lambda / 2\pi r^2$ where r is the radius of the eye.
33
34 514 As shown in Figure 2, all light from the illuminated area of the retina that exits the pupil is
35
36 515 transmitted through the pupil; that is the light reflected back through the pupil is not Lambertian
37
38 516 and so the output of a pixel corresponding to an image of the pupil is
39
40
41
42
43
44

$$45 \quad 46 \quad 47 \quad 517 \quad v_p = \frac{\eta a_p L_0^\lambda}{2\pi r^2} 10^{-2\varepsilon^\lambda cl} \quad (2)$$

48
49 518 where the exponential term corresponds to application of the Beer-Lambert law, e' is the
50
51 519 extinction coefficient of blood at wavelength λ and l is the thickness of the choroid. The ODR
52
53 520 for measurements recorded at wavelengths λ_1 and λ_2 is therefore given by
54
55
56
57
58
59
60

$$521 \quad ODR = \frac{\log_{10} \frac{v_p^{l_1}}{v_c^{l_1}}}{\log_{10} \frac{v_p^{l_2}}{v_c^{l_2}}} = \frac{X^{a_{p,l_1}} - e^{l_1} cl}{X^{a_{p,l_2}} - e^{l_2} cl} \quad (3)$$

522 where

$$523 \quad X^{a,l} = \log_{10} \left(\frac{a}{2A' (r\rho N_i)^2} \right) \quad (4)$$

524 We employ spectrally neutral calibration tiles so $A^{l_1} = A^{l_2}$ and due to mydriasis a can be
 525 assumed constant during the experiments and $X^{a_{p,l}}$ can be considered as a constant, ξ . Taking
 526 the log of ratio of $v_p^{l_1}/v_c^{l_1}$ to $v_p^{l_2}/v_c^{l_2}$ yields

$$527 \quad cl = \frac{OD^{\lambda_1} - OD^{\lambda_2}}{\varepsilon^{\lambda_2} - \varepsilon^{\lambda_1}} \quad (5)$$

528 which can be substituted into (6) to yield

$$529 \quad e^{l_2} = e^{l_1} \frac{OD^{l_2} - X}{OD^{l_1} - X} \quad (6)$$

530 We choose λ_2 to be an isosbestic point, such as 800 nm, and λ_1 to be an oxygen-sensitive
 531 wavelength such as 780 nm and substitute $e^{l_1} = s e_{HbO}^{l_1} + (1-s) e_{Hb}^{l_1}$, where s is optical saturation and
 532 the subscripts HbO and Hb denote the extinction coefficients for oxygenated and deoxygenated
 533 haemoglobin respectively there is a proportionate relationship between s and ODR:

$$534 \quad s = \frac{1}{e_{HbO}^{780} - e_{Hb}^{780}} \left(e^{l_2} \frac{OD^{780} - \frac{X}{OD^{800}}}{1 - \frac{X}{OD^{800}}} - e_{HbO}^{l_1} \right) \quad (7)$$

$$= m \cdot ODR + c$$

536 where

$$537 \quad m = \frac{e^{l_2}}{(e_{HbO}^{780} - e_{Hb}^{780}) \left(1 - \frac{X}{OD^{800}}\right)} \quad (8)$$

$$538 \quad c = -\frac{e^{l_2}}{e_{HbO}^{780} - e_{Hb}^{780}} \left(\frac{X}{OD^{800} - X} + \frac{e_{HbO}^{l_1}}{e^{l_2}} \right) \quad (9)$$

539 Note that ξ varies with a_p and so both the gradient and offset of this relationship are sensitive
 540 to variations in the pupil diameter.